Hindawi Publishing Corporation
International Journal of Photoenergy
Volume 2013, Article ID 129621, 10 pages
http://dx.doi.org/10.1155/2013/129621

Research Article

Effects of Surface Modification of TiO_2 Nanotube Arrays on the Performance of CdS Quantum-Dot-Sensitized Solar Cells

Danhong Li, Nengqian Pan, Jianjun Liao, Xiankun Cao, and Shiwei Lin

Key Laboratory of Ministry of Education for Advanced Materials in Tropical Island Resources, School of Materials and Chemical Engineering, Hainan University, Haikou 570228, China

Correspondence should be addressed to Shiwei Lin; linsw@hainu.edu.cn

Received 17 January 2013; Revised 3 April 2013; Accepted 5 April 2013

Academic Editor: Maria da Graça P. Neves

CdS-sensitized TiO_2 nanotube arrays have been fabricated using the method of successive ionic layer adsorption and reaction and used as a photoanode for quantum-dot-sensitized solar cells. Before being coated with CdS, the surface of TiO_2 nanotube arrays was treated with $TiCl_4$, nitric acid (HNO_3), potassium hydroxide (KOH), and methyltrimethoxysilane (MTMS), respectively, for the purpose of reducing the interface transfer resistance of quantum-dot-sensitized solar cells. The surfaces of the modified samples represented the characteristics of superhydrophilic and hydrophobic which directly affect the power conversion efficiency of the solar cells. The results showed that surface modification resulted in the reduction of the surface tension, which played a significant role in the connectivity of CdS and TiO_2 nanotube arrays. In addition, the solar cells based on CdS/TiO_2 electrode treated by HNO_3 achieved a maximum power conversion efficiency of 0.17%, which was 42% higher than the reference sample without any modification.

1. Introduction

Since the new architecture for the dye-sensitized solar cell (DSSC) was first reported by O'Regan and Grätzel in 1991, it has attracted considerable attention throughout the world from both academic and industrial fields as one of promising candidates for the development of next generation solar cells [1–5]. DSSCs use dyes to sensitize wide band gap semiconductors to convert visible light into electricity, while quantum-dot-sensitized solar cells (QDSSCs) generally use quantum dots (QDs) as sensitized materials instead of conventional organic dyes [6, 7]. Accordingly, semiconductor QDs as light absorbing materials have many fascinating advantages, such as their high extinction coefficients and large intrinsic dipole moment that originated from bulk properties [8, 9]. Besides, the tunable band gap by size controlling and multiple excition generation by impact ionization are derived from the nanoscale dimension as a consequence of the quantum confinement effect [10–12]. However, the quantum-dot-sensitized solar cells have shown comparatively much lower efficiencies than expected and have not been fully systematically explored and evaluated.

To date, one-dimensional TiO_2 nanostructures, particularly TiO_2 nanotube arrays (TNAs), have received great attention in terms of quantum-dot-sensitized solar cells. A large surface area facilitates the creation of a large number of junctions and an increase in the amount of sensitizer material that can be loaded on the TiO_2 surface, thereby leading to favorable light harvesting and collection of photogenerated charge carriers [13]. Additionally, the tubular architecture and vertical orientation of TNAs facilitate the separation of the photoexcited charges and accelerate electron transport [14]. However, at present, the record solar conversion efficiencies of QDSSCs based on TNAs are lower than 5%. QDSSCs based on the CdSe/CdS-sensitized TNAs/Ti photoanode and Cu_2S counterelectrode just had a performance of 3% which was lower than 7% achieved from colloid quantum dot solar cells [14, 15]. Kamat et al. linked CdSe QDs to TiO_2 with bifunctional organic molecules and successfully increased the power conversion efficiency of solar cell due to the acceleration of the electron injection rate from CdSe to TiO_2 [16, 17]. Thus, interface properties greatly influence the interfacial electron transfer process. Surface modification via different approaches, such as surface modification with

molecular dipoles and coating quantum-dot-sensitized TNAs with ZnS nanometric barriers, has been demonstrated to be a powerful tool to boost the power conversion efficiencies of the devices [18–20].

In our previous work, we reported the effects of geometric and crystal structures on the photoelectrical properties of TNAs and the enhanced photoelectrochemical property of nitrogen-doped TNAs [21, 22]. In this paper, we investigated the effects of interfacial properties on the QDSSCs performances through surface modification of TiO_2 nanotube arrays. After the modification, the nanotube surfaces showed a superhydrophilic or superhydrophobic behavior, which resulted from various surface tensions. Despite the vast reports on QDSSCs, there is little research on the influence of the characteristics of surface superhydrophilic and superhydrophobic as well as surface tensions. Therefore, we modified the surface of TNAs by $TiCl_4$, nitric acid (HNO_3), and potassium hydroxide (KOH), respectively, to change the surface tension of the TNAs. Subsequently, CdS quantum dots were deposited by the method of successive ionic layer adsorption and reaction (SILAR). After modification, 0.17% power conversion efficiency was achieved by treatment of HNO_3, which was 42% higher than the reference solar cell.

2. Experimental

2.1. Preparation and Modification of TiO_2 Nanotube Arrays. Ti foil (0.5 mm thickness, 99.4% purity) was first cut into 1.5 cm × 3 cm. The foils were ultrasonically cleaned in acetone, ethanol, and deionized water for 30 min, respectively, and dried in ambient air. The Ti foil was anodized in ethylene glycol solution containing 0.3 wt% NH_4F and 2 wt% H_2O by applying a 60 V DC potential for 4 h. The anodization was performed in a two-electrode configuration with the Ti foil as the working electrode and a stainless steel foil as the counterelectrode. After anodization, the TNAs on Ti foil were ultrasonically treated in ethanol for 5 min to remove the electrolyte and debris on top, followed by thermal treatment at 450°C for 3 h. Then the samples were soaked in $TiCl_4$ (0.04 M), HNO_3 (pH = 3), and KOH (pH = 12), respectively, for 30 min at 70°C. And the sample soaked in $TiCl_4$ subsequently re-annealed at 450°C for 30 min.

2.2. Deposition of CdS QDs. The CdS-sensitized TiO_2 photoanodes were achieved by SILAR of CdS QDs on TNAs. The as-prepared photoanodes were firstly immersed into a solution of 0.05 M $Cd(NO_3)_2$ in ethanol for 2 min, then rinsed with ethanol, and then immersed into 0.05 M Na_2S in methanol/water (1 : 1/v : v) for another 2 min, followed by another rinsing with deionized water and methanol. Such an immersion cycle was repeated 8 times until the desired deposition of CdS QDs was achieved. The sensitized photoanodes were passivated with ZnS by alternately dipping into 0.5 M $Zn(NO_3)_2$ ethanol solution and 0.5 M Na_2S methanol/water solution three times for 2 min for each time.

2.3. Fabrication of Counterelectrodes and Solar Cells Assembly. To assemble the solar cell, a Pt-coated counterelectrode was prepared by dropping 5 mM H_2PtCl_6 in isopropanol onto FTO glass and then annealed at 385°C for 30 min. The cells were assembled in a sandwiched structure with a thermal adhesive film (Surlyn, 60 μm, DuPont). A methanol/water (7 : 3 by volume) solution containing 0.5 M Na_2S, 2 M S, and 0.2 M KCl was used as the redox electrolyte. The electrolyte was injected by vacuum backfilling, and then the hole was sealed with a Surlyn film. The effective area of the cell is 0.3 cm^2.

2.4. Characterization. The morphology and microstructure of the photoanodes were characterized by scanning electron microscopy (FESEM, Hitachi S-4800) and transmission electron microscopy (TEM, JOEL JEM2100), and the crystal structure was studied by X-ray diffraction measurements (XRD, Bruker AXS, D8 Advance). The absorption spectrum was obtained by a UV-vis spectrophotometer (Persee, TU-1901). The current and voltage measurements were recorded by Keithley 2400 sourcemeter when the cells were irradiated by a solar simulator (Aulight, CEL-S500) under AM 1.5 illumination of 100 mW/cm^2. All the electrochemical impedance spectroscopy (EIS) measurements of QDSSCs were carried out in dark and under the open circuit potentials. The superimposed signal has the frequency ranging from 0.1 Hz to 100 KHz with AC amplitude of 10 mV (Zahner, Zennium).

3. Results and Discussion

3.1. Contact Angle Analysis. The top-view and side-view images of highly ordered TNAs prepared by anodic oxidation are shown in Figure 1(a). The tube length is measured to be 20 μm while the average inner diameter 150 nm. To observe the surface characteristics of the resulting surfaces, modified TNAs were investigated by equilibrium contact-angle measurements. The TNAs without any surface modification were used as a reference, and the corresponding contact angle is displayed in Figure 1(b). The water contact angle is 6.3 ± 2°, and the surface is practically wetting and represents a superhydrophilic behavior. We doubt that the reason for the phenomenon of the surface derives from the spreading water on the entire surface and into the pores [23]. Figures 1(c)–1(e) exhibit the contact angles of TNAs modified by $TiCl_4$, HNO_3, and KOH, respectively, and the resulting contact angles are 12.2 ± 2°, 1.2 ± 2°, and 9.4 ± 2°, respectively. It can be seen that the contact angles are different and the TNAs treated by HNO_3 represent the best hydrophilicity. Besides the reason that water is spreading into the pores which is similar to the reference sample, the changes of active site and surface property play a key role in the surface wetting behavior of the TNAs modified with HNO_3. Moreover, notice that the contact angles of modified samples are similar to that of the reference, all of which are smaller than 50° and show a superhydrophilic behavior. In order to study the effect of the superhydrophilic/superhydrophobic surface on the QDSSCs performance, a TNAs sample was modified with also methyltrimethoxysilane (MTMS) which is usually used for surface hydrophobic modification. The

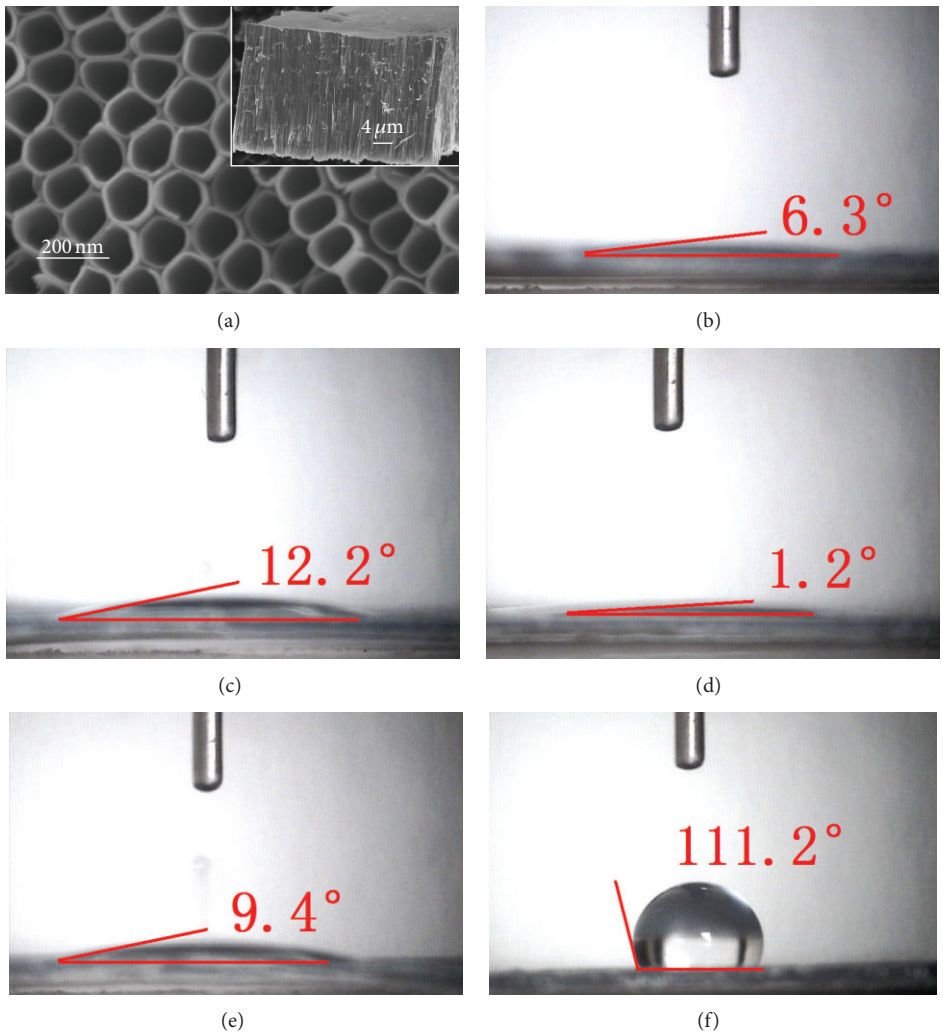

FIGURE 1: (a) Top-view SEM image of the TNAs with the corresponding side-view image in the inset. (b) Contact angle of the reference TNAs sample. Contact angles of the TNAs modified by (c) $TiCl_4$, (d) HNO_3, (e) KOH, and (f) MTMS.

originally superhydrophilic surface becomes hydrophobic with a contact angle of about 111.2±2° as shown in Figure 1(f).

3.2. Morphological Analysis. Figure 2 shows the top-view and side-view SEM images of CdS-sensitized TiO_2 nanotube arrays. In Figure 2(a), CdS quantum dots are well distributed on the top surface of the TNAs without any modification, while some CdS quantum dots are found to aggregate on the openings of TNAs. The side-view SEM image in Figure 2(a) depicts that the vast majority of QDs are found to aggregate and attach to the external tube wall. The results indicate that because of the effect of surface tension, the CdS precursor solutions could not penetrate deeply into the nanotubes and cause large aggregation of CdS on the top surface and external tube wall [24]. Figure 2(b) represents the great majority of CdS quantum dots aggregated in the openings of TiO_2 nanotubes treated by $TiCl_4$. The side-view SEM image shows that CdS QDs are located on the inner tube wall of TNAs and distributed uniformly. As depicted in Figure 2(c), CdS QDs treated by HNO_3 are homogeneous and rarely aggregate in the openings. Moreover, the distribution of CdS QDs in the inner spaces is also uniform and few aggregated as illustrated in the inset of Figure 2(c). In Figure 2(d), a great majority of CdS QDs aggregate in the openings of TNAs treated by KOH, while the side-view image shows a similar distribution of the sample treated by $TiCl_4$. In the case of MTMS-treated TNAs shown in Figure 1(e), large quantity of CdS QDs blocked in the surface openings, and the side-view image in inset shows a uniform distribution in the inner spaces of TNAs. According to the surface characteristics in Figure 1, the results shown in Figure 2 suggest that superhydrophilic surface might have a uniform QDs distribution, while hydrophobic surface might be easy to cause QDs aggregation.

To further clarify whether or not the CdS QDs are introduced into the nanotubes wall under the influence of hydrophilic and hydrophobic modification of TNAs coated with CdS, the samples were investigated by TEM. Figure 3 shows TEM images of the reference sample and CdS/TNAs treated by $TiCl_4$, HNO_3, KOH, and MTMS, respectively. As shown in Figure 3(a), few CdS QDs are deposited in

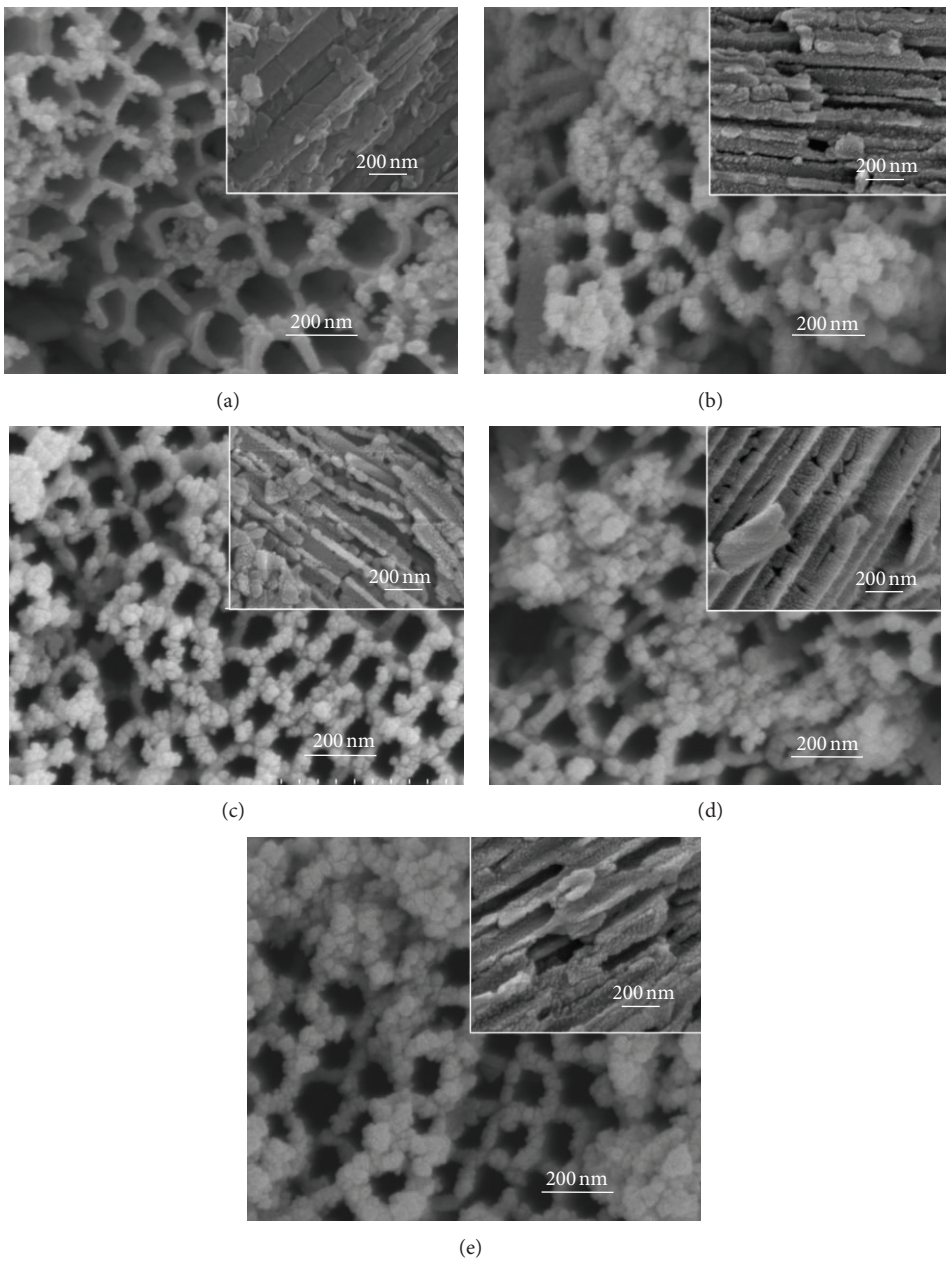

Figure 2: (a) Top-view and side-view images of the CdS/TNAs and the TNAs modified by (b) $TiCl_4$, (c) HNO_3, (d) KOH, and (e) MTMS.

the nanotube wall of the reference sample without surface treatment. Compared with the reference sample, many CdS QDs have been attached to the nanotube wall of the sample treated by $TiCl_4$ which is shown in Figure 3(b). And the CdS QDs are found to be aggregated in the tube wall. After being treated by HNO_3, as depicted in Figure 3(c), a great majority of CdS QDs deposited in nanotube wall are better distributed. In addition, the sizes of QDs are more uniform. Similarly, the CdS QDs are also found to be aggregated for the HNO_3-treated sample. As shown in Figure 3(d), CdS QDs apparently aggregate together for the CdS/TiO_2 electrode treated by KOH. Besides, the CdS/TNAs electrode modified by MTMS represents the phenomenon of aggregation and the nonuniform distribution of CdS QDs in Figure 3(e). By combining Figures 2 and 3, we suggest that the CdS QDs are more uniformly distributed on the tube wall of TNAs after the treatment of HNO_3 because of its superhydrophilic characteristic and smaller surface tension. Close observation by high-resolution TEM demonstrates that the size of CdS QDs is about 5–10 nm in diameter, as depicted in Figure 3(f).

3.3. XRD Analysis. The crystal structure of the deposited CdS was examined by X-ray diffraction experiments. For comparison, the X-ray diffraction pattern from the TNAs sample is also given as curve 1 in Figure 4, where diffraction peaks are the anatase phase of TiO_2 (JCPDS card no. 21-1272) and Ti metal phase. Curves 2–6 represent the diffraction peaks of CdS/TNAs treated without and with $TiCl_4$,

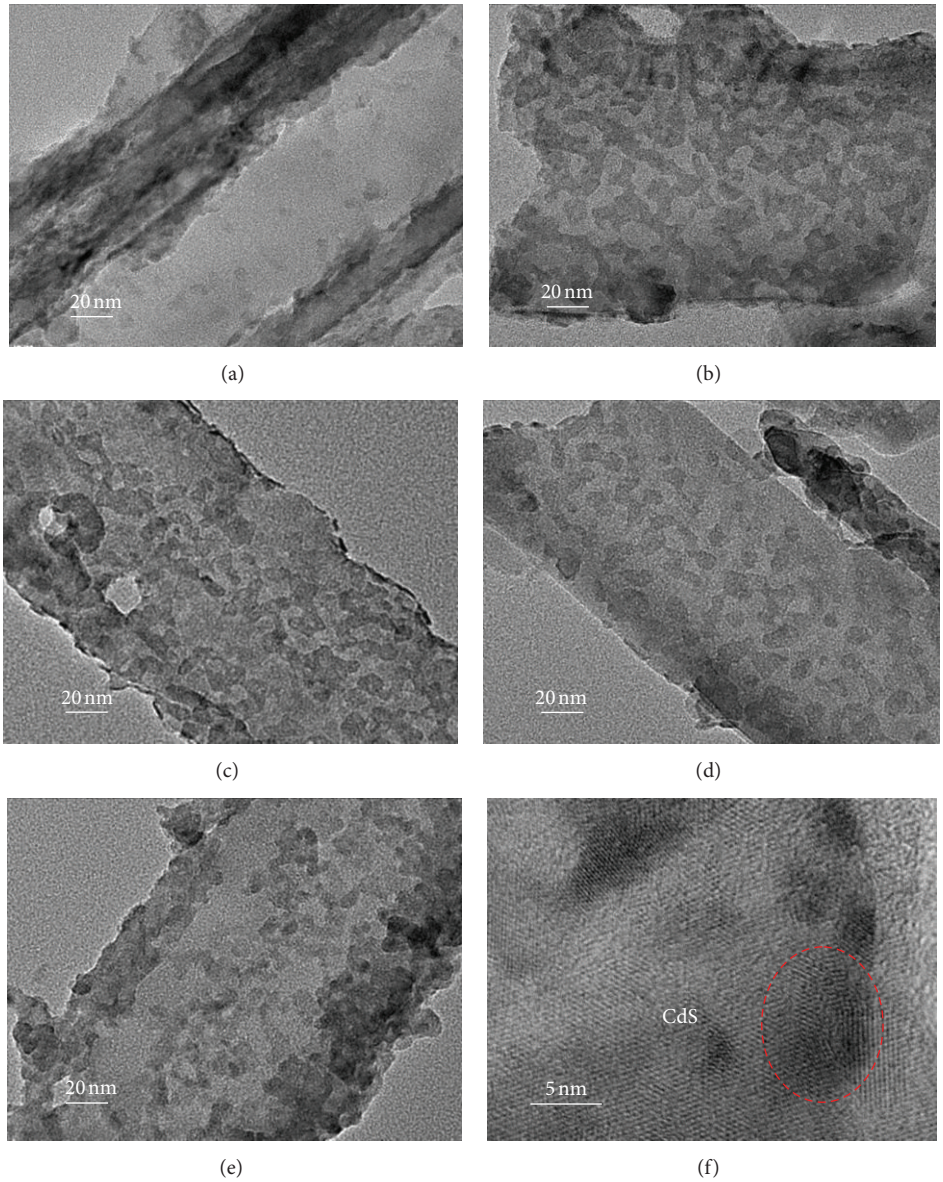

Figure 3: TEM images of (a) CdS/TNAs without surface treatment and CdS/TNAs treated by (b) $TiCl_4$, (c) HNO_3, (d) KOH, (e) MTMS, and (f) correspond to high-resolution TEM image of HNO_3-modified CdS/TNAs.

HNO_3, KOH, and MTMS, respectively. Compared to the TiO_2 nanotubes arrays, CdS/TNAs electrodes exhibited new peaks corresponding to (111), (220), (331) planes of CdS, indicating the presence of the cubic phase CdS (JCPDS card no. 80-0019). The XRD patterns of CdS/TNAs electrodes with different treatments are quite similar, which suggests that surface modification could not change the crystal structure of the photoanode.

3.4. UV-Vis Absorption Spectra Analysis. Figure 5(a) shows the UV-vis absorption spectra of the pure TiO_2 nanotube arrays, pure CdS particles, and CdS-sensitized TNAs without any treatment and treated with $TiCl_4$, HNO_3, KOH, and MTMS, respectively. The TNAs sample does not exhibit absorption in the visible light region, although it shows absorption in the UV light region. While compared with the TNAs absorption spectrum, an apparent absorption peak in the visible light region exists for the pure CdS particles, which can be attributed to its narrow band gap properties. Moreover, from Figure 5(b), it can be found that the absorption edge of the CdS appears at about 530 nm by the method of linear extrapolation, which is just making the tangent in the starting absorption point to get the absorption edge. Then the band gap of CdS could be calculated. Since spectra are typically reported in units corresponding to the wavelength of light rather than its energy, the conversion between conventional wavelength and band gap energy units can be carried out by the equation described below [25]:

$$h\nu\,(\mathrm{eV}) = \frac{1239.8\,(\mathrm{eV}\times\mathrm{nm})}{\lambda\,(\mathrm{nm})}. \quad (1)$$

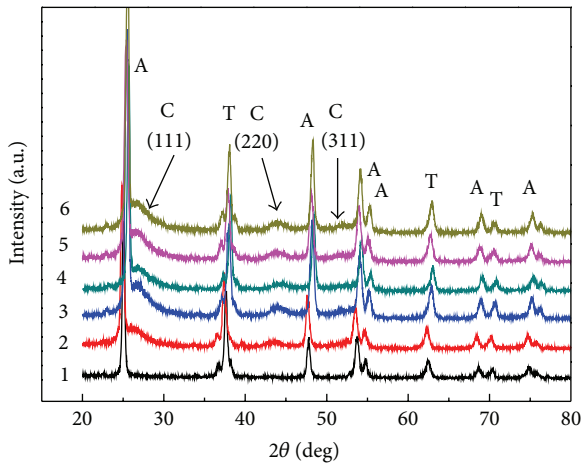

FIGURE 4: XRD patterns of CdS/TNAs without modification (curve 2) and modified with $TiCl_4$ (curve 3), HNO_3 (curve 4), KOH (curve 5), and MTMS (curve 6), respectively. Curve 1 refers to the XRD pattern of the reference TNAs sample.

Herein, the band gap of the pure CdS is 2.34 eV. As depicted in Figure 5(a), curve 1 is the absorption spectrum of reference CdS/TNAs electrode. A considerable absorbance in the visible light region can be observed, and the absorption peak is ascribed to the loading of the CdS nanoparticles. In addition, the absorption spectrum of the CdS/TiO_2 electrode in 400 to 550 nm is very similar to that of the pure CdS. It is implied that CdS QDs have a synergism on TNAs, which basically enhance the absorption intensity in the visible light region in comparison with the pure TNAs. While in the range between 550 and 750 nm, the absorption spectrum of reference electrode is the same as that of TNAs, suggesting that TNAs act synergistically on CdS QDs. Besides, the inhabitation of CdS QDs within the TNAs is beneficial for maintaining more reaction active sites [26]. Curves 2–5 are CdS/TNAs electrodes with the treatment of $TiCl_4$, HNO_3, KOH, and MTMS, respectively. The absorption spectra of these electrodes are similar to that of the reference. And the spectra are close to each other due to the similar CdS particle sizes and CdS contents. From Figures 5(c)–5(e), it can be observed that the band edges of reference electrode and CdS/TiO_2 electrodes treated with HNO_3 and MTMS are 520 nm, 520 nm, and 530 nm, respectively. The corresponding band gaps are about 2.38 eV, 2.38 eV, and 2.34 eV on the basis of (1), which are all slightly higher than that of the bulk CdS (2.25 eV). Furthermore, the sizes of the CdS particles on the TNAs are still within the scale of QDs [27, 28], which have already been testified by the HRTEM image in Figure 3(f). As depicted in Figures 5(c)–5(e), the absorption edges of reference sample and HNO_3-treated electrode are a little lower than that of MTMS-treated sample. Furthermore, the results are in line with that of Figure 2 since the CdS QDs deposited in the reference sample and HNO_3-treated TNAs are more uniformly distributed than other electrodes.

3.5. Photovoltaic Performance and Charge Transfer. The *J-V* curves of QDSSCs treated without and with $TiCl_4$, HNO_3, KOH, and MTMS are shown in Figure 6. The open circuit potential (V_{oc}), short circuit current density (J_{sc}), fill factor (FF), and conversion efficiency (η) of all cells are listed in Table 1. The J_{sc} and V_{oc} of the reference electrode are 0.943 mA/cm^2 and 0.37 V, respectively, resulting in a very low value of conversion efficiency of 0.12%. And the effect of the $TiCl_4$ treatment TNAs is also evaluated using the same parameters. An increase in the J_{sc} of $TiCl_4$-treated solar cell is observed in Table 1, while the efficiency of the cell represents a small decrease due to the reduction of the V_{oc} and FF. The lower V_{oc} is possibly ascribe to the decrease of the electrons transported from CdS QDs to TiO_2 conduction band, leading to a decrease in the quasi-Fermi level of TiO_2 [29], while lower FF may be attributed to the low driving force for the electron injection [29]. Moreover, these results clearly reflect that the $TiCl_4$ treatment does not have a beneficial effect on QDSSCs. In the case of HNO_3-treated solar cell, a systematic beneficial effect is observed. The J_{sc}, V_{oc}, and η are 1.460 mA/cm^2, 0.36 V, and 0.17%, respectively. The efficiency of 0.17% is 42% higher than that of the reference solar cell. Accordingly, the higher J_{sc} seems to be mostly owing to the better connectivity between TNAs and CdS QDs. This implies that the strong oxidizing property and high acidity of the HNO_3 to some extent help make better contact between TNAs and CdS QDs [30]. Therefore, well-connected structures are able to promote electron transfer and improve J_{sc}. For the solar cell treated with KOH, the photovoltaic performance is similar to the $TiCl_4$-treated solar cell. The J_{sc} is higher while V_{oc} and FF are lower than those of the reference cell. In addition, the MTMS-treated solar cell shows lower V_{oc} and efficiency than that of the reference cell. These results are in good agreement to that of Figures 2 and 3, and the lower efficiencies of the solar cells are due to the blocking QDs in the opening of nanotubes. Moreover, the J_{sc} of HNO_3-treated solar cell increases to a maximum value of 1.460 mA/cm^2, which is possibly because of the increase amount of CdS QDs deposited on TiO_2 and the uniform distribution of the QDs.

In order to find out the reasons why J_{sc} increases in the photoanode after HNO_3 treatment, we further investigated the electron transport and charge recombination processes of the solar cells by applying EIS. Figure 7 shows the Nyquist plots and Bode plots of CdS-sensitized solar cells modified with and without HNO_3, respectively, which are measured under dark conditions and open circuit potentials. EIS is a useful technique to detect kinetic processes in QDSSCs. Two distinct arcs of each plot could be seen from Figure 7(a), representing the electron transport processes at the interface of TNAs/CdS/electrolyte (frequency region 1–1000 Hz) and the feature of polysulfide solution diffusion in the electrolyte (<1 Hz). Generally, the plots of QDSSCs exhibit three arcs, while in our case the interface of the counterelectrode/electrolyte is not so obvious in the frequency region 1–100 kHz which is shown in the inset of Figure 7(a). The electrochemical parameters obtained from equivalent circuit analysis are presented in Table 2. The equivalent circuit of the solar cells is represented in

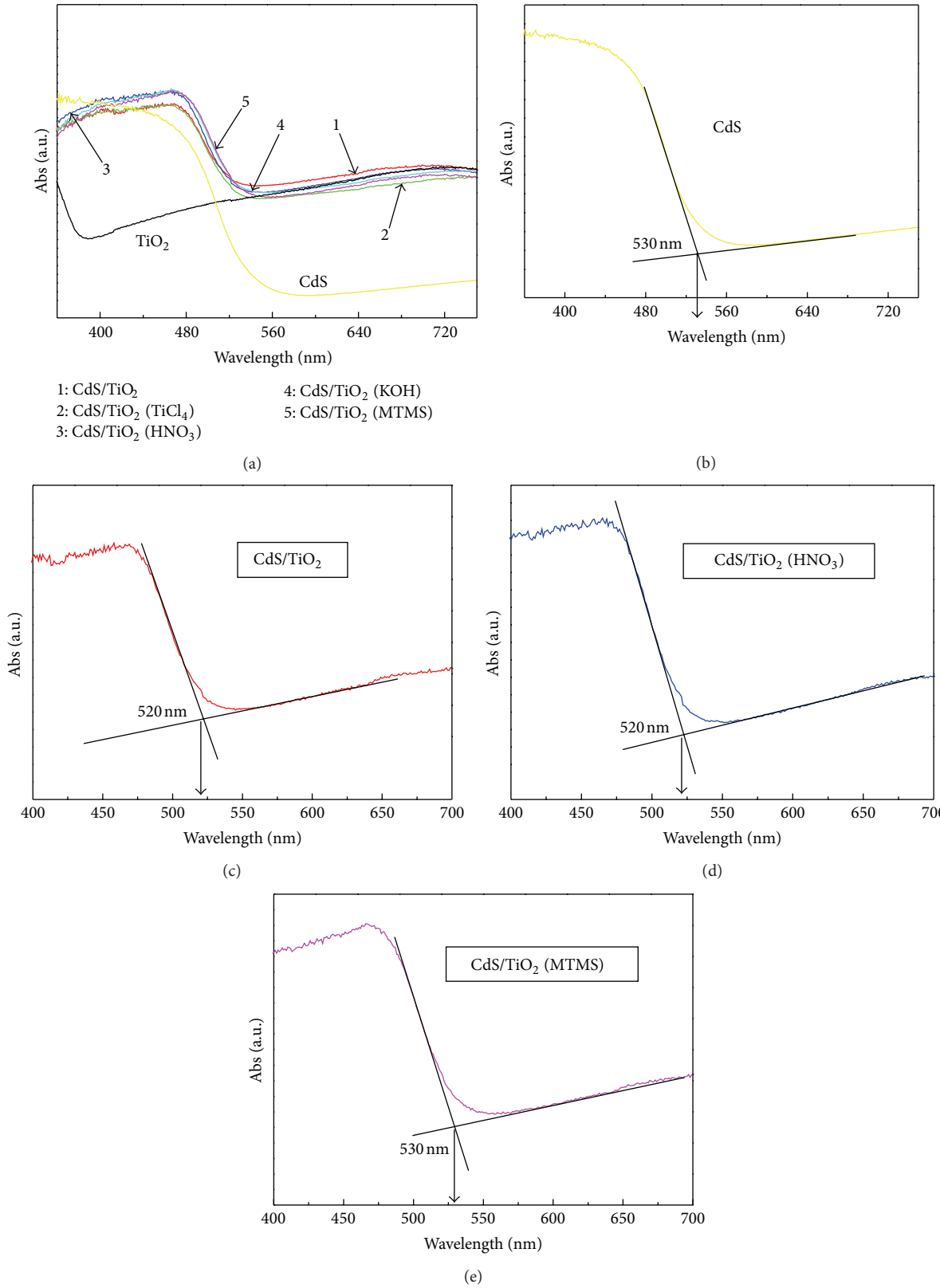

Figure 5: (a) UV-vis absorption spectra of TiO_2 nanotube arrays and CdS/TNAs with different modifications. Linear extrapolation is conducted to get absorption edges of (b) CdS particles, (c) CdS/TiO_2, and (d) CdS/TiO_2 treated with HNO_3 and (e) CdS/TiO_2 treated with MTMS.

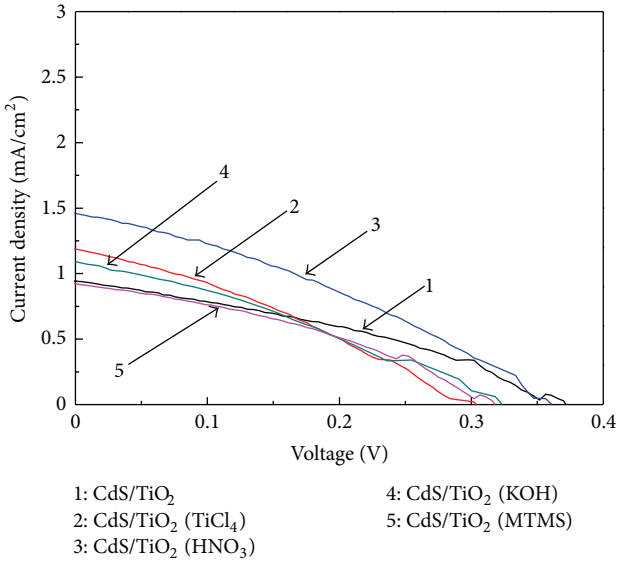

Figure 6: J-V curves of CdS-sensitized solar cells with different modifications.

Table 1: Photovoltaic parameters of QDSSCs with different modifications.

Sample	J_{sc} (mA/cm^2)	V_{oc} (V)	FF	η (%)
CdS/TiO$_2$	0.943	0.37	0.35	0.12
CdS/TiO$_2$ (TiCl$_4$)	1.188	0.30	0.31	0.11
CdS/TiO$_2$ (HNO$_3$)	1.460	0.36	0.34	0.17
CdS/TiO$_2$ (KOH)	1.169	0.32	0.31	0.12
CdS/TiO$_2$ (MTMS)	0.923	0.32	0.36	0.11

the inset of Figure 7(b). For relatively low resistance, the transfer resistance of counterelectrode/electrolyte interface does not play a key role in the whole resistance of solar cell. Therefore, charge transfer is dominated by the transfer resistance at the interface of TNAs/CdS/electrolyte and the diffusion resistance of electrolyte. From Table 2, it can be seen that the values of R_{CT2} and R_E for reference and HNO$_3$-treated solar cells are 62.45 and 180.4 Ω, 37.04 and 127.1 Ω, respectively. It is inferred that HNO$_3$-treated solar cell shows a lower charge transfer resistance which is responsible for the observed higher photocurrent density (J_{sc} = 1.460 mA/cm^2) compared to reference sample. And the results are in good agreement with the photovoltaic performance of solar cells shown in Figure 6. This phenomenon may be due to the better hydrophilicity and lower surface tension of the solar cells treated by HNO$_3$. Moreover, because of the decrease of excessive CdS hindering the access of electrolyte deep into the inner tube, J_{sc} of the HNO$_3$ treatment solar cells is larger than other cells. Correspondingly, the characteristic frequency peaks in Bode phase plots are shown in Figure 7(b).

4. Conclusions

In summary, CdS-sensitized TiO$_2$ nanotube arrays have been fabricated by successive ionic layer adsorption and reaction

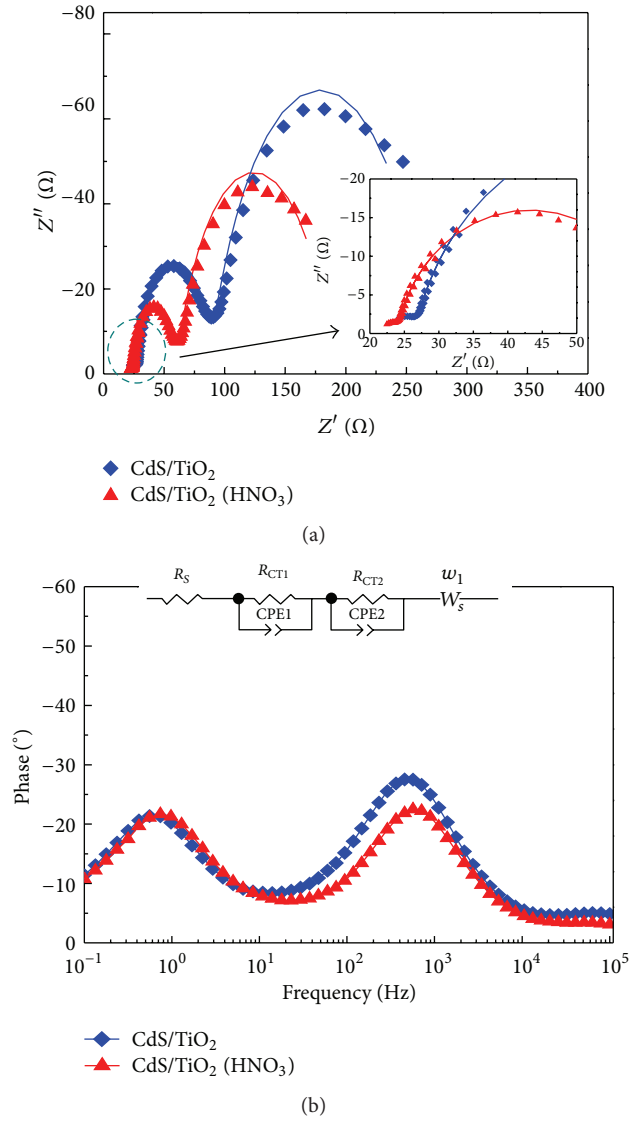

Figure 7: Electrochemical impedance spectra of CdS-sensitized solar cells: (a) Nyquist plots and (b) Bode plots.

Table 2: Electrochemical parameters of reference and HNO$_3$-treated solar cells.

Sample	R_s (Ω)	R_{CT1} (Ω)	R_{CT2} (Ω)	R_E (Ω)
CdS/TiO$_2$	22.98	3.596	62.45	180.4
CdS/TiO$_2$ (HNO$_3$)	21.85	2.09	37.04	127.1

and applied as the photoanode for quantum dots solar cells, in which the TNAs were modified using TiCl$_4$, HNO$_3$, KOH, and MTMS, respectively, The experimental results indicated that the conversion efficiency of HNO$_3$-treated electrode was apparent higher than that of the solar cells without any modification, which resulted from the large surface coverage and the uniform distribution of the CdS quantum dots. Furthermore, reducing surface tension leads to a better adsorption and combination and the obvious decrease of

interface transfer impedance. As a consequence, the HNO_3-treated solar cells achieve a maximum short current density of 1.460 mA/cm^2 and a power conversion efficiency of 0.17%, which is 42% higher than the reference sample without any surface modification.

Acknowledgments

This work was supported by Program for New Century Excellent Talents in University (NCET-09-0110), National Nature Science Foundation of China (51162007), Hainan Natural Science Foundation (511110), and Hainan Provincial Program for International S&T Cooperation (KJHZ2013-13). The authors acknowledge Mr. Guizhen Wang for the analysis of transmission electron microscopy in the Analytical and Testing Center of Hainan University. They also acknowledge Professor Hong Lin at Tsinghua University for the help of fabrication and characterization of the solar cells.

References

[1] B. O'Regan and M. Grätzel, "A low-cost, high-efficiency solar cell based on dye-sensitized colloidal TiO_2 films," *Nature*, vol. 353, pp. 737–740, 1991.

[2] Y. H. Jang, X. K. Xin, M. Byun, Y. J. Jang, Z. Q. Lin, and D. H. Kim, "An unconventional route to high-efficiency dye-sensitized solar cells via embedding graphitic thin films into TiO_2 nanoparticle photoanode," *Nano Letters*, vol. 12, no. 1, pp. 479–485, 2012.

[3] Q. Zhang, X. Guo, X. Huang et al., "Highly efficient CdS/CdSe-sensitized solar cells controlled by the structural properties of compact porous TiO_2 photoelectrodes," *Physical Chemistry Chemical Physics*, vol. 13, no. 10, pp. 4659–4667, 2011.

[4] G. Zhu, L. Pan, T. Xu, Q. Zhao, B. Lu, and Z. Sun, "Microwave assisted CdSe quantum dot deposition on TiO_2 films for dye-sensitized solar cells," *Nanoscale*, vol. 3, no. 5, pp. 2188–2193, 2011.

[5] A. Braga, S. Giménez, I. Concina, A. Vomiero, and I. Mora-Seró, "Panchromatic sensitized solar cells based on metal sulfide quantum dots grown directly on nanostructured TiO_2 electrodes," *Journal of Physical Chemistry Letters*, vol. 2, no. 5, pp. 454–460, 2011.

[6] S. H. Im, Y. H. Lee, S. I. Seok, S. W. Kim, and S. W. Kim, "Quantum-dot-sensitized solar cells fabricated by the combined process of the direct attachment of colloidal CdSe quantum dots having a ZnS glue layer and spray pyrolysis deposition," *Langmuir*, vol. 26, no. 23, pp. 18576–18580, 2010.

[7] E. M. Barea, M. Shalom, S. Giménez et al., "Design of injection and recombination in quantum dot sensitized solar cells," *Journal of the American Chemical Society*, vol. 132, no. 19, pp. 6834–6839, 2010.

[8] A. Salant, M. Shalom, Z. Tachan, S. Buhbut, A. Zaban, and U. Banin, "Quantum rod-Sensitized solar cell: nanocrystal shape effect on the photovoltaic properties," *Nano Letters*, vol. 12, no. 4, pp. 2095–2100, 2012.

[9] Y. L. Lee and Y. S. Lo, "Highly efficient quantum-dot-sensitized solar cell based on co-sensitization of CdS/CdSe," *Advanced Functional Materials*, vol. 19, no. 4, pp. 604–609, 2009.

[10] Y. C. Park, E. H. Kong, Y. J. Chang, B.-G. Kum, and H. M. Jang, "Tertiary hierarchically structured TiO_2 for CdS quantum-dot-sensitized solar cells," *Electrochimica Acta*, vol. 56, no. 21, pp. 7371–7376, 2011.

[11] P. Sudhagar, J. H. Jung, S. Park, R. Sathyamoorthy, H. Ahn, and Y. S. Kang, "Self-assembled CdS quantum dots-sensitized TiO_2 nanospheroidal solar cells: structural and charge transport analysis," *Electrochimica Acta*, vol. 55, no. 1, pp. 113–117, 2009.

[12] H. Wang, Y. Bai, H. Zhang, Z. Zhang, J. Li, and L. Guo, "CdS quantum dots-sensitized TiO_2 nanorod array on transparent conductive glass photoelectrodes," *Journal of Physical Chemistry C*, vol. 114, no. 39, pp. 16451–16455, 2010.

[13] C. Li, J. Yuan, B. Han, L. Jiang, and W. Shangguan, "TiO_2 nanotubes incorporated with CdS for photocatalytic hydrogen production from splitting water under visible light irradiation," *International Journal of Hydrogen Energy*, vol. 35, no. 13, pp. 7073–7079, 2010.

[14] X. F. Guan, S. Q. Huang, Q. X. Zhang et al., "Front-side illuminated CdS/CdSe quantum dots co-sensitized solar cells based on TiO_2 nanotube arrays," *Nanotechnology*, vol. 22, no. 46, Article ID 465402, 2011.

[15] A. H. Ip, S. M. Thon, S. Hoogland, and E. H. Sargent, "Hybrid passivated colloidal quantum dot solids," *Nanotechnology*, vol. 127, no. 7, pp. 557–582, 2012.

[16] I. Robel, V. Subramanian, M. Kuno, and P. V. Kamat, "Quantum dot solar cells. Harvesting light energy with CdSe nanocrystals molecularly linked to mesoscopic TiO_2 films," *Journal of the American Chemical Society*, vol. 128, no. 7, pp. 2385–2393, 2006.

[17] P. V. Kamat, K. Tvrdy, D. R. Baker, and J. G. Radich, "Beyond photovoltaics: semiconductor nanoarchitectures for liquid-junction solar cells," *Chemical Reviews*, vol. 110, no. 11, pp. 6664–6688, 2010.

[18] H. J. Lee, J. Bang, J. Park, S. Kim, and S. M. Park, "Multilayered semiconductor (CdS/CdSe/ZnS)-sensitized TiO_2 mesoporous solar cells: all prepared by successive ionic layer adsorption and reaction processes," *Chemistry of Materials*, vol. 22, no. 19, pp. 5636–5643, 2010.

[19] M. Seol, E. Ramasamy, J. Lee, and K. J. Yong, "Highly efficient and durable quantum dot sensitized ZnO nanowire solar cell using noble metal-free counter electrode," *The Journal of Physical Chemistry C*, vol. 115, no. 44, pp. 22018–22024, 2011.

[20] Y. L. Lee, C. F. Chi, and S. Y. Liau, "CdS/CdSe Co-Sensitized TiO_2 photoelectrode for efficient hydrogen generation in a photoelectrochemical cell," *Chemistry of Materials*, vol. 22, no. 3, pp. 922–927, 2010.

[21] D. H. Li, S. W. Lin, S. P. Li, X. Huang, X. K. Cao, and J. B. Li, "Effects of geometric and crystal structures on the photoelectrical properties of highly ordered TiO_2 nanotube arrays," *The Journal of Materials Research*, vol. 27, no. 7, pp. 1029–1036, 2012.

[22] S. P. Li, S. W. Lin, J. J. Liao, N. Q. Pan, D. H. Li, and J. B. Li, "Nitrogen-doped TiO_2 nanotube arrays with enhanced photoelectrochemical property," *International Journal of Photoenergy*, vol. 2012, Article ID 794207, 7 pages, 2012.

[23] E. Balaur, J. M. MacAk, L. Taveira, and P. Schmuki, "Tailoring the wettability of TiO_2 nanotube layers," *Electrochemistry Communications*, vol. 7, no. 10, pp. 1066–1070, 2005.

[24] L. Yang, S. Luo, R. Liu et al., "Fabrication of cdse nanoparticles sensitized long TiO_2 nanotube arrays for photocatalytic degradation of anthracene-9-carbonxylic acid under green monochromatic light," *Journal of Physical Chemistry C*, vol. 114, no. 11, pp. 4783–4789, 2010.

[25] J. D. Dow and D. Redfield, "Electroabsorption in semiconductors: the excitonic absorption edge," *Physical Review B*, vol. 1, no. 8, pp. 3358–3371, 1970.

[26] M. Samadpour, P. P. Boix, S. Giménez et al., "Fluorine treatment of TiO_2 for enhancing quantum dot sensitized solar cell performance," *Journal of Physical Chemistry C*, vol. 115, no. 29, pp. 14400–14407, 2011.

[27] Y. L. Lee, B. M. Huang, and H. T. Chien, "Highly efficient CdSe-sensitized TiO_2 photoelectrode for quantum-dot-sensitized solar cell applications," *Chemistry of Materials*, vol. 20, no. 22, pp. 6903–6905, 2008.

[28] S. C. Hayden, N. K. Allam, and M. A. El-Sayed, "TiO_2 nanotube/CdS hybrid electrodes: extraordinary enhancement in the inactivation of escherichia coli," *Journal of the American Chemical Society*, vol. 132, no. 41, pp. 14406–14408, 2010.

[29] J. Chen, D. W. Zhao, J. L. Song et al., "Directly assembled CdSe quantum dots on TiO_2 in aqueous solution by adjusting pH value for quantum dot sensitized solar cells," *Electrochemistry Communications*, vol. 11, no. 12, pp. 2265–2267, 2009.

[30] P. P. Boix, G. Larramona, A. Jacob, B. Delatouche, and J. Bisquert, "Hole transport and recombination in all-solid Sb2S3-sensitized TiO_2 solar cells using CuSCN as hole transporter," *The Journal of Physical Chemistry C*, vol. 116, no. 1, pp. 1579–1587, 2012.